Science Bulletin xxx (xxxx) xxx

Contents lists available at ScienceDirect

Science Bulletin

journal homepage: www.elsevier.com/locate/scib

Article

Distinctive South and East Asian monsoon circulation responses to global warming

Tim Li [a,b,*], Yuhao Wang [a], Bin Wang [b], Mingfang Ting [c], Yihui Ding [d], Ying Sun [d], Chao He [e], Guang Yang [b]

[a] Collaborative Innovation Center on Forecast and Evaluation of Meteorological Disasters/Key Laboratory of Meteorological Disaster, Ministry of Education/Joint International Research Laboratory of Climate and Environmental Change, Nanjing University of Information Science and Technology, Nanjing 210044, China
[b] International Pacific Research Center and Department of Atmospheric Sciences, School of Ocean and Earth Science and Technology, University of Hawaii at Manoa, Honolulu HI 96822, USA
[c] Lemont-Doherty Earth Observatory, Columbia University, Palisades, NY 10964, USA
[d] National Climate Center, Beijing 100081, China
[e] Institute for Environmental and Climate Research, Jinan University, Guangzhou 511400, China

ARTICLE INFO

Article history:
Received 23 July 2021
Received in revised form 10 November 2021
Accepted 12 November 2021
Available online xxxx

Keywords:
Global warming
South and East Asian monsoon circulation changes
Fast and slow responses
Tibetan Plateau
Sea surface temperature warming pattern

ABSTRACT

The Asian summer monsoon (ASM) is the most energetic circulation system. Projecting its future change is critical for the mitigation and adaptation of billions of people living in the region. There are two important components within the ASM: South Asian summer monsoon (SASM) and East Asian summer monsoon (EASM). Although current state-of-the-art climate models projected increased precipitation in both SASM and EASM due to the increase of atmospheric moisture, their circulation changes differ markedly—A robust strengthening (weakening) of EASM (SASM) circulation was projected. By separating fast and slow processes in response to increased CO_2 radiative forcing, we demonstrate that EASM circulation strengthening is attributed to the fast land warming and associated Tibetan Plateau thermal forcing. In contrast, SASM circulation weakening is primarily attributed to an El Niño-like oceanic warming pattern in the tropical Pacific and associated suppressed precipitation over the Maritime Continent.

1. Introduction

The Asian summer monsoon (ASM) is the most energetic monsoon system around the globe [1]. The large-scale monsoon circulation brings abundant moisture from the tropical ocean to the continent and supplies more than half of the annual rainfall [2]. The variability of the monsoon rainfall could cause natural disasters such as floods or droughts and exert a profound impact on agriculture and economy [3]. Unravelling the mechanisms controlling the monsoon change in a warmer climate is a demanding task, which is of great societal and economic value.

As reported by Intergovernmental Panel on Climate Change (IPCC) Fifth Assessment Report (AR5) [4], the ASM rainfall was projected to increase in the future warmer climate. This increase was explained by the "wet-get-wetter" [5,6] or the "richest-get-richer" mechanism [7], due to the increase of moisture caused by the surface warming. However, much greater uncertainty exists in the projection of the monsoon circulation among the state-of-the-art climate models [8–10], because the circulation change involves more complicated processes including the changes of atmospheric static stability [11–13], land–ocean thermal contrast [14,15], orographic effects [16–18], and sea surface temperature (SST) pattern [13,19,20].

The ASM consists of two important sub-systems, South Asian summer monsoon (SASM) characterized by a pronounced low-level westerly and East Asian summer monsoon (EASM) characterized by a pronounced low-level southerly [21] (Fig. S1 online). While the SASM westerly was projected to weaken under global warming [9,22–24], the EASM southerly was projected to strengthen [22,25,26]. What causes such distinctive circulation changes? Turner and Annamalai [9] argued that the weakening of SASM was caused by the increase of atmospheric static stability. If this is true, one may wonder why this mechanism does not work in EASM. On the other hand, the cause of the strengthened EASM circulation was argued to be caused by an enhanced land-sea thermal contrast [22,25,26], as the Eurasian continent warms faster than the ocean [25,27]. If this is the case, one may wonder why the heated Eurasian continent does not strengthen the westerly in SASM. Motivated by the controversial arguments above, we intend to resolve the outstanding science issue, namely, what are

* Corresponding author.
E-mail address: timli@hawaii.edu (T. Li).

https://doi.org/10.1016/j.scib.2021.12.001
2095-9273/

the fundamental mechanisms responsible for the distinctive monsoon circulation changes.

A climate response to increased greenhouse gas forcing involves two processes—A fast process and a slow process [8,28–30]. The former is the fast adjustment of the land and atmosphere to the intensified radiative forcing due to increased greenhouse gas concentration, with the timescale of days to weeks [28,31]. The latter is referred to a slow SST change with the timescale of tens or hundreds of years [32,33], depending on geographic location. It has been shown that both the direct radiative forcing and the slow SST adjustment exert a great impact on the tropical and extratropical climate [8,28,30,34]. By separating the monsoon climate response to a fast and a slow response, one can identify the fundamental mechanism for the monsoon climate change under global warming. In the current study, we investigate specific processes through which the fast and the slow processes modulate the ASM circulation and their relative roles. A special attention will be paid to the effects of Tibetan Plateau (TP) thermal forcing and the future SST warming pattern in monsoon circulation changes.

2. Methods

2.1. Model and observational data, projection method and fast and slow processes

The monthly output from the following experiments performed by the CMIP6 models is adopted for analyses: (1) The Historical (HIST) experiment from 30 CMIP6 models, in which the coupled models are forced by the historical forcing [35]. The latter half of the 20th period (1950–1999) in the HIST experiment is defined as the baseline climate (20C). (2) The future climate experiment under the SSP5-8.5 scenario (SSP5-8.5) from the same 30 CMIP6 models, in which the radiative forcing towards 8.5 W m^{-2} at the year of 2100 [35]. The latter half of the 21th period (2050–2099) is defined as the future warmer climate (21C). The 21C is compared against the 20C to investigate the change of ASM under greenhouse warming. The adoption of the high emission scenario and the long-term (50 years rather than 20 years used in AR5) climate average could sufficiently suppress the impact of the internal variability and the global warming forced climate response can be largely extracted [36–38]. (3) To investigate the relative role of the fast and slow processes in modulating the ASM, the Preindustrial-Control (PIC) and abruptly quadrupling CO_2 (abrupt-4 × CO_2) experiments from 42 coupled general circulation models (CGCMs) participating in CMIP6 are further adopted. The PIC experiment is performed with the fixed external forcing at preindustrial level, and is integrated for hundreds years [35]. The abrupt-4 × CO_2 is a branch experiment from the PIC simulation, in which the CO_2 concentration is quadrupling that at preindustrial level and the model is integrated for 150 years [35]. Following previous studies [28,39], as the SST change is negligible in the first year due to the large thermal inertia, the fast response is defined by the difference between the first year in the abrupt-4 × CO_2 experiment and the last 50-year average in the PIC experiment. As the SST adjusts slowly to the radiative forcing, the slow response is defined as the difference between the last 50-year average and the first year in the abrupt-4 × CO_2 experiment. The detailed information about all the CMIP6 models adopted in the current study is listed in Table S1 (online).

The multi-model ensemble median (MMM) is used to evaluate the forced climate response instead of the multi-model mean, for the median is more robust to the outliers [40,41]. For each model, all the changes are scaled by the global mean surface temperature (GMST) warming before the MMM is taken, to evaluate the climate change per degree warming and remove the possible impact from the climate sensitivity [19,38]. For comparison, 30 CMIP5 model (HIST and RCP8.5) outputs are also used, and the adopted CMIP5 models are same as in Wang et al. [12]. All the model data are interpolated onto a 2.5° × 2.5° horizontal grid before analysis. We also examine the main results with higher interpolation resolution (1° × 1°, 1.75° × 1.75°). The spatial pattern and the magnitude of the ASM change under different interpolation resolution are generally same (Figs. 1 and S2 online). Since the large-scale feature of the SASM and EASM is focused on, the choice of the interpolation resolution in a reasonable range does not destroy the robustness of the results in the current study.

To depict the observational feature of the ASM, monthly wind data from the National Centers for Environmental Prediction – Department of Energy (NCEP-DOE) reanalysis [42] and the Global Precipitation Climatology Project (GPCP) monthly precipitation dataset [43] from the period 1979–2008 are also used.

2.2. Definition of monsoon metrics

To quantitatively measure the change of the SASM and EASM circulation, two sets of the monsoon circulation metrics are used. The SASM metrics consist of the following three indices: (1) South Asian summer monsoon index (SASMI) is defined as the box-averaged 850 hPa zonal wind (2.5°−15°N, 55°−100°E; blue box in Fig. 1). The dominant circulations in both the upper and lower troposphere over South Asia (SA) all occur in the blue box region (Fig. S1 online), and the SASMI is adopted to directly measure the change of the intensity of the climatological maximum westerly. (2) Vertical wind shear (VWS) index is defined as the box-averaged (2.5°−15°N, 55°−100°E; blue box in Fig. 1) zonal wind difference between 850 and 200 hPa following Webster and Yang [44], which reflects both the strength of the lower and upper tropospheric zonal wind and the north–south land-sea thermal contrast. (3) Meridional wind shear (MWS) index (MWS1) is defined as 850 hPa zonal wind difference between (5°–15°N, 40°–80°E) and (20°–30°N, 70°–90°E) following Wang et al. [45], which is more closely related to the variation of the SASM rainfall [45].

The EASM metrics consist of the following three indices: (1) East Asian summer monsoon index (EASMI) is defined as the box-averaged 850 hPa southerly over East Asia (EA; 20°–45°N, 110°–125°E; blue box in Fig. 1) to directly measure the intensity of the climatological southerly [22,26,39]. (2) Following Guo [46], Zonal SLP gradient index (SLPG) is defined as zonal SLP difference between the mid-latitude North Pacific (25°–50°N, 130°E–150°W) and the Eurasian Continent (25°–50°N, 30°–110°E), to measure the east–west land-sea thermal contrast. (3) Meridional wind shear index (MWS2) is defined as 850 hPa zonal wind difference between (22.5°–32.5°N, 110°–140°E) and (5°–15°N, 90°–130°E) following Wang et al. [47], which well reflects the variation of the rainfall over EA [47].

Their specific definitions are listed as follow:

SASMI = U850(2.5°–15°N, 55°–100°E),
VWS = U850(2.5°–15°N, 55°–100°E) – U200(2.5°–15°N, 55°–100°E),
MWS1 = U850(5°–15°N, 40°–80°E) – U850(20°–30°N, 70°–90°E),
EASMI = V850(20°–45°N, 110°–125°E),
SLPG = SLP(25°–50°N, 130°E–150°W) – SLP(25°–50°N, 30°–110°E),
MWS2 = U850(22.5°–32.5°N, 110°–140°E) – U850(5°–15°N, 90°–130°E),

where U850 and U250 denote the zonal wind at 850 and 200 hPa respectively, V850 denotes the meridional wind at 850 hPa, and SLP represents the sea level pressure.

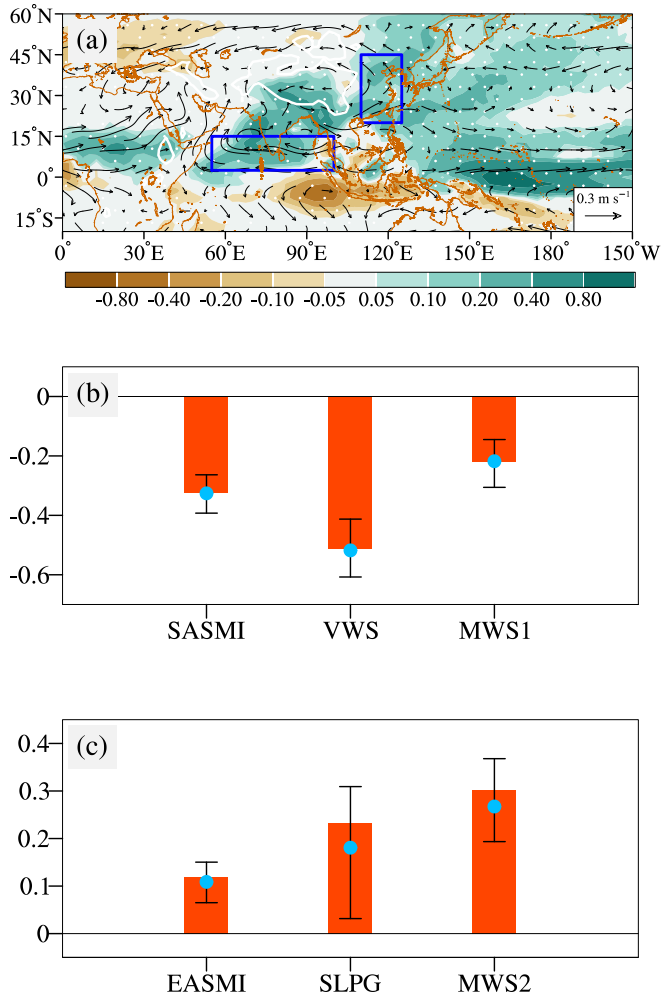

Fig. 1. Projected changes of ASM under global warming. (a) Projected changes of the precipitation (shading, mm d^{-1}) and 850 hPa wind (vector, m s^{-1}) in the SSP5-8.5 experiment relative to the HIST experiment. All the changes are scaled by the global mean surface temperature (GMST) warming, and the changes agreed in sign by at least 70% of the individual models are stippled. The blue rectangles denote the key region for the EASM (20°–45°N, 110°–125°E) and SASM (2.5°–15°N, 55°–100°E). White contours denote the topography. (b), (c) Changes of SASM and EASM monsoon metrics respectively. The SASM metrics include SASMI (m s^{-1}), VWS (×2 m s^{-1}) and MWS1 (m s^{-1}). The EASM metrics include EASMI (m s^{-1}), SLPG2 (×10^2 Pa) and MWS2 (m s^{-1}). The detailed definition for each monsoon metric is described in Methods. The color bar is the MMM, the blue dot represents the multi-model ensemble mean (MME), and the whisker denotes the range between the 30th and 70th percentiles of the individual models.

2.3. An anomaly atmospheric general circulation model

To investigate the impact of a heating anomaly on the monsoon circulation, an anomaly atmospheric general circulation model is used. This anomaly model is developed based on the Geophysical Fluid Dynamics Laboratory (GFDL) global spectral dry AGCM (atmospheric general circulation model) [48]. A seasonal mean flow is specified as the model background state. For more details of this anomaly model, readers are referred to Jiang and Li [49] and Li [50]. This anomaly model has been used to examine the atmospheric circulation response to a prescribed MJO (Madden-Julian oscillation) heating over the eastern Indian Ocean (IO) [49], the instability of synoptic-scale wave trains over the tropical western North Pacific [50], and the response of El Niño induced circulation anomaly to global warming [12]. For each simulation, the model is integrated for 120 d, and the last 40-d result is used to depict the steady response to the prescribed heating.

3. Results

Fig. 1a shows the change of low-level wind and precipitation in boreal summer (June-July-August, JJA) projected by CMIP6 models in terms of multi-model median (MMM). Rainfall increases robustly over South Asia (SA) and East Asia (EA), while it decreases over the equatorial eastern IO and the Maritime Continent (MC). In contrast to the consistent rainfall increase over SA and EA, the pronounced circulation changes distinctively between the two regions. Easterlies appear over the SASM domain (blue box, 55°–100°E, 2.5°–15°N, a region of maximum climatological westerlies in summer as seen in Fig. S1 online), implying a weakening of SASM circulation. The easterly anomalies turn southward to form an anticyclonic flow south of the equator and turn northward and eastward over the Indian subcontinent, leading to an intensified westerly over the southern TP. Given the negative heating anomaly over the MC, the anomalous circulation pattern over the IO is reminiscent of the typical pattern of the Gill response [51]. Southerlies prevail over EA, indicating the strengthening of the EASM circulation. Over the Eurasian continent, the circulation change is characterized by an anomalous large-scale cyclone, ranging from 20° to 60°N and from 10° to 120°E. The general feature of the projected circulation changes in terms of multi-model ensemble mean (MME) and in the CMIP5 model projection is similar (Fig. S3 online), indicating that they are a robust signal.

To quantitatively measure the change of SASM and EASM circulation, the two sets of defined monsoon metrics are used. The projected changes of the SASM and EASM metrics for the CMIP6 models are shown in Fig. 1b, c respectively. For SASM, all three indices consistently project a robust and significant weakening signal, with a weakened westerly accompanied by weakened vertical and meridional shears (Fig. 1b; Table S2 online). For EASM, a projected strengthening of low-level southerly is accompanied by significantly enhanced zonal SLP gradient and meridional wind shear (Fig. 1c; Table S2 online). The quantitatively analyses based on the monsoon metrics further demonstrate a robust weakened SASM circulation and a robust strengthened EASM circulation under global warming.

Next we investigate the physical mechanisms responsible for the distinctive circulation changes, by decomposing the climate response into a fast and a slow process. The detailed definitions of the fast and slow processes are referred to the Methods.

The fast response to the direct CO_2 radiative forcing is shown in Fig. 2a. While rainfall over the Asian and African monsoon regions increases, low-level wind weakens over SA but strengthens over EA. This differs markedly from the slow response to the SST (Fig. 2b), which shows a weakening of low-level wind in both the EASM and SASM regions.

The sum of the fast and slow responses is depicted in Fig. 2c. The changes of the rainfall and circulation patterns in Fig. 2c resemble well the CMIP6 projected changes shown in Fig. 1a. While the summer rainfall increases in both EASM and SASM, the monsoonal wind weakens over SA but strengthens over EA. The pattern similarity suggests that the decomposition of the fast and slow responses to global warming based on the PIC and abrupt-4 × CO_2 experiment is reasonable.

Fig. 2d further reveals the relative role of the fast and slow processes in affecting the SASM and EASM circulation change. While only SASMI and EASMI are shown here, a similar conclusion is obtained with the other indices (Table S2 and Fig. S4 online). The significant weakening of SASMI is to a large extent attributed to the slow oceanic process, whereas the strengthening of EASMI is primarily attributed to the fast land warming process.

How does the fast process intensify the EASM circulation while the slow ocean process weaken it? To examine the fast response to

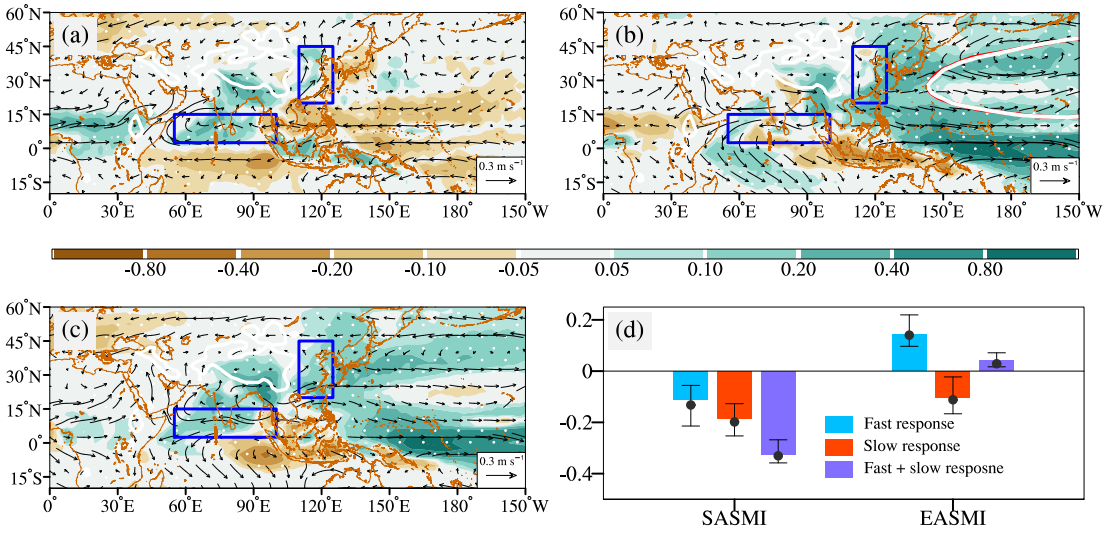

Fig. 2. Changes of ASM in the fast and slow responses. The change of precipitation (shading, mm d^{-1}) and 850 hPa wind (vector, m s^{-1}) in the fast (a) and slow (b) responses to the abruptly quadrupling of CO_2. (c) Same as (a) and (b) but for the sum of the fast and slow responses. All the changes are scaled by the GMST warming, and the changes agreed in sign by at least 70% of the individual models are stippled. White contours denote the topography. The red and white curves in (b) denote the location of the North Pacific subtropical high (NPSH) in the PIC simulation and the slow response respectively, denoted by the zero contour of the eddy geopotential height (H_e) which is calculated by removing the zonal mean geopotential height over the 0°–40°N. (d) Changes of the SASMI (m s^{-1}) and EASMI (m s^{-1}) in the fast and slow responses and their sum. The color bar is the MMM, the black dot represents the MME, and the whisker denotes the range between the 30th and 70th percentiles of the individual models.

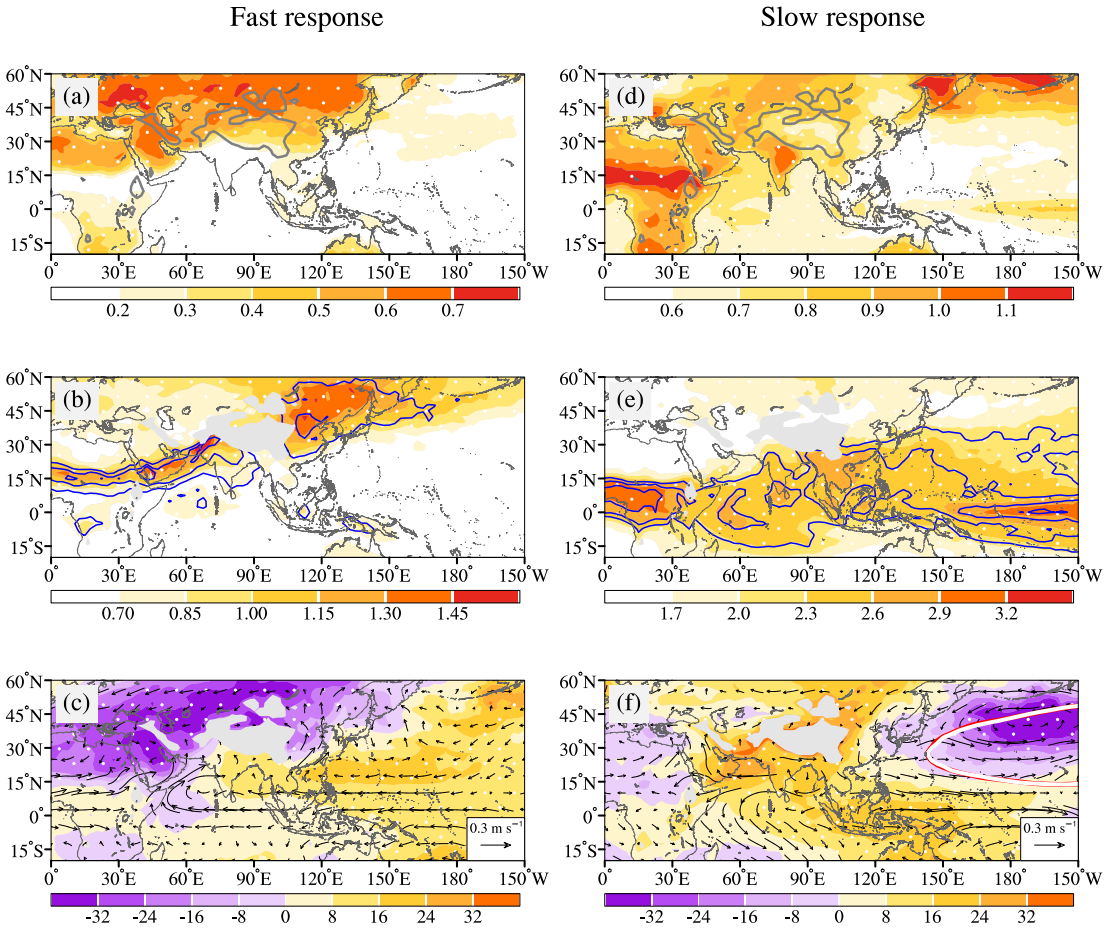

Fig. 3. Changes of thermal features in the fast and slow responses. Left panel: the change of (a) surface temperature (TS; K), (b) equivalent potential temperature (θ_e; shading, K) and specific humidity (contour; g kg^{-1}) at 850 hPa, and (c) sea level pressure (SLP; shading, Pa) and horizontal wind (vector, m s^{-1}) at 850 hPa in the fast response. All the changes are scaled by the GMST warming, and the changes agreed in sign by at least 70% of the individual models are stippled. Right panel is same as left panel but for the slow response. The contours in (b) are from the 0.2 to 0.6 g kg^{-1} with the interval of 0.1 g kg^{-1}, and the contours in (e) are from the 0.5 to 0.8 g kg^{-1} with the interval of 0.1 g kg^{-1}. The red and white curves over the North Pacific shown in (f) are same as that in Fig. 2b.

direct CO_2 radiative forcing, we plotted the change of surface temperature in Fig. 3a. A marked feature is the rapid warming over land while the ocean SST change is negligible. This is because the ocean response to the radiative forcing is much slower due to its larger heat capacity compared to land [27]. This enlarges the zonal land-sea thermal contrast between the Asian continent and the Pacific to its east, which is a key driver for the EASM circulation [22,25,26]. Under the direct increased CO_2 radiative forcing, a marked warming appears over the Eurasian continent (Fig. 3a). The warming results in a large-scale anomalous cyclone at 850 hPa with an enhanced southerly over EA, accompanied by a negative SLP anomaly over the Eurasia continent (Fig. 3c). The southerly transports higher mean moisture from the tropical ocean, leading to an increase of specific humidity and equivalent potential temperature (θ_e) over EA (Fig. 3b), favoring the setup of a convectively unstable stratification *in situ*, which increases local precipitation (Fig. 2a).

While the result above supports the notion that the zonal land–ocean thermal contrast in the fast response contributes to the intensification of the southerly EASM, it is interesting to note that the enhanced southerly occurs primarily in boreal summer while the Eurasian land warming appears throughout the year (Fig. S5 online). This implies that as part of the land–ocean thermal contrast in boreal summer, TP thermal forcing may play an important role. It has been shown that the TP thermal forcing is a major heat source in northern hemispheric summer and is critical for pushing the EASM rain band and southerly beyond 40°N [17,18,52]. Observational evidences demonstrate that the summertime TP thermal forcing is primarily contributed by the surface sensible heating and the column latent heating associated with the precipitation [17,52]. While under global warming, change of the TP thermal forcing is dominated by the latent heating associated with the change of precipitation (Fig. S6 online). Thus the precipitation over the TP (25°–37.5°N, 75°–102.5°E; red box in Fig. S6 online) is adopted as the proxy for the TP thermal forcing [16]. The monthly evolution of the precipitation changes over the TP and southerly over EA is further plotted in Fig. S5b (online), to examine the effect of the TP thermal forcing. Note that they show high consistency, that is, an enhanced southerly appears primarily in boreal summer when the TP thermal forcing is intensified. Scatter diagrams between the EASMI and the TP thermal forcing among 30 CMIP6 SSP5-8.5 and 42 abrupt-4 × CO_2 experiments confirm the relationship (Fig. 4a, c). Physically, an intensified TP thermal forcing can induce a cyclonic low-level flow surrounding the TP [16,52], strengthening EASM southerly. The result above indicates that the fast land warming and associated TP thermal forcing play an important role in strengthening the EASM circulation.

The weakened EASM southerly in the slow response is caused by a weakened North Pacific subtropical high (NPSH) (Fig. 3f). In contrast to a positive zonal SLP gradient in the fast process (Fig. 3c), a negative zonal SLP gradient appears north of 15°N in the slow response (Fig. 3f). The change of the large-scale zonal pressure gradient is fundamentally caused by the tropical and mid-latitude ocean warming (Fig. 3d). In the tropics, the ocean warming is characterized by an El Niño-like warming over the equatorial Pacific and an Indian Ocean Dipole (IOD)-like warming over the IO. Although the amplitude of the tropical and mid-latitude ocean warming is smaller than that over the land, its impact on the atmospheric moisture and convective activity is much greater. As shown in Fig. 3e, a much greater increase of the low-level specific humidity and θ_e occurs over most of the tropical and mid-latitude oceans. The change of θ_e overlays with the change of specific humidity (Fig. 3e), implying the θ_e change is primarily determined by the moisture change. The increased low-level θ_e over the Pacific causes the increase of local convective instability and thus precipitation over the climatological mean ascending regions [53,54] (Fig. 2b). As a result, the NPSH weakens (see a quantitative analysis of the NPSH intensity change in Fig. S7c online) and an anomalous cyclone appears over the subtropical North Pacific [39] (Fig. 3f). It is worth mentioning that the location of the NPSH remains unchanged (see red and white curves in Fig. 2b and 3f and a quantitative evaluation of the NPSH center and western boundary locations in Fig. S7d online). This suggests that the weakening of the NPSH intensity is the main signal in the slow response.

What causes the weakening of SASM circulation? As shown in Fig. 2d, the weakening is to a large extent attributed to the slow oceanic process. An El Niño-like warming pattern appears in the equatorial Pacific (Fig. 3d). The cause of this warming pattern is possibly attributed to a longwave radiative and evaporative damping mechanism [55] and/or an enhanced equatorial westerly associated with a strengthened western North Pacific monsoon (South Pacific Convergence Zone) in boreal summer (winter) [56]. The El Niño-like warming pattern leads to suppressed precipitation over MC (Fig. 2b), which further induces a Rossby wave response with an anticyclonic circulation pattern over the IO [51,57] (Fig. 2b). As a result, a pronounced easterly anomaly appears over the SA box (Fig. 2b). The IOD warming pattern may further strengthen the easterly anomaly. Scatter diagrams between the SASMI and the mean SST change in the equatorial central-eastern Pacific among 30 CMIP6 SSP5-8.5 and 42 abrupt-4 × CO_2 experiments illustrate a significant relationship between them (Fig. 4b, d), confirming the SASM circulation—SST relationship.

To illustrate the impact of the negative precipitation anomaly over the MC on SASM circulation, we conducted an idealized numerical experiment with an anomaly AGCM (see Methods). A negative heating anomaly is prescribed over the MC (10°S–10°N, 90°–130°E) with a maximum heating rate of 1 K d^{-1} (Fig. 5a). A pronounced easterly anomaly is reproduced over the SA box, accompanied by two anomalous anticyclone gyres as part of the Rossby wave response. The ridge of the anomalous anticyclone points toward India, favoring a weakening of SASM [57]. The idealized simulation demonstrates the essential role of the suppressed precipitation over the MC in weakening the SASM circulation in association with the slow SST response.

One remaining question is why SASM circulation weakens in the fast response (Fig. 2a), given large-scale land warming and negative SLP anomalies over Eurasia (Fig. 3a, c). As seen in Fig. 2a, a positive rainfall anomaly appears over North Africa (NA). The rainfall over NA may induce a Kelvin wave response with easterly anomalies over the northern IO, which may push the land warming induced westerly northward to the southern TP. The increase of the NA rainfall results from the convective instability *in situ*, as seen from zonally oriented specific humidity and equivalent potential temperature anomaly fields in NA (Fig. 3b). The rainfall anomaly shifts slightly to the south as the climatological mean NA monsoon precipitation is located to the south of 15°N. The increases of the local moisture and θ_e arise from the moisture transport by southwesterly flow, which is a part of the large-scale cyclonic flow over Eurasia (Fig. 3c). It is the competition of the NA rainfall effect and the large-scale land warming over Eurasia that leads to a low-level anticyclone over India (Fig. 2b), with easterly (westerly) anomalies south (north) of 15°N. A scatter diagram between SASMI and NA rainfall changes in the fast response shows a significant relationship (Fig. S8 online).

To investigate the impact of the intensified NA rainfall, we conducted another set of the anomaly AGCM experiment with a specified heating (same maximum heating rate of 1 K d^{-1}) over NA (0°–20°N, 0°–55°E). Fig. 5b shows the simulation result. A cyclonic anomaly is stimulated over the North Atlantic, whereas easterly anomalies are induced over the northern IO. Therefore, the numer-

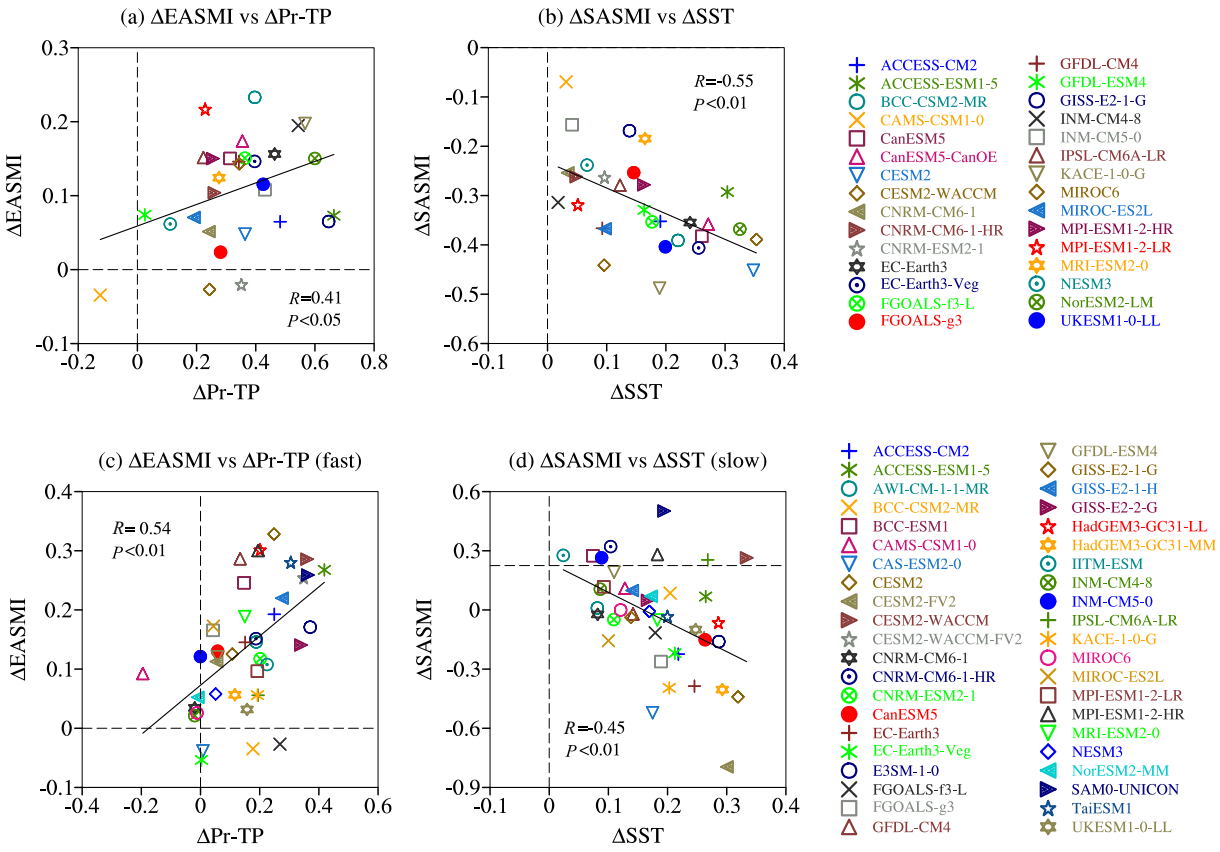

Fig. 4. Inter-model relationships between ASM circulation changes and TP thermal forcing/SST warming pattern. Scatter diagrams for (a) the EASMI change (m s^{-1}) and the precipitation change over TP (25°–37.5°N, 75°–102.5°E; mm d^{-1}) and for (b) the SASMI change (m s^{-1}) and the mean SST change (K) over the equatorial central-eastern Pacific (2.5°S–2.5°N, 160°–90°W) in the SSP5-8.5 experiment relative to the HIST experiment. (c), (d) Same as in (a) and (b), but for the fast and slow responses respectively. The SST in (b) and (d) is derived by removing the tropical (30°S–30°N) mean SST.

ical experiment supports the hypothesis that the increased NA rainfall weakens the SASM circulation.

4. Conclusion and discussion

By diagnosing the CMIP6 model outputs, we revealed physical mechanisms responsible for the distinctive circulation changes over SASM and EASM under global warming. The CMIP6 models consistently projected a strengthened EASM circulation but a weakened SASM circulation in the future warmer climate state. Through examining the monsoon circulation responses to fast and slow processes respectively, the primary drivers for the change of the SASM and EASM circulation are identified.

Fig. 6 is a schematic diagram illustrating the key processes. In response to increased CO_2 radiative forcing (with the timescale of days to weeks), the Eurasian continent warms quickly while the ocean remains unchanged (Fig. 6a). The fast land warming over Eurasia, along with the TP thermal forcing, induces large-scale low SLP and cyclonic circulation, strengthening the low-level southerly over EA. Meanwhile, an enhanced rainfall appears over North Africa, due to moisture transport by anomalous southwesterly. This positive rainfall anomaly over NA induces anomalous easterly over the northern IO, resulting in the weakening of the SASM circulation.

A slow oceanic response (with the timescale of tens or hundreds of years) to the radiative forcing leads to an El Niño-like warming pattern in the equatorial Pacific (Fig. 6b). This warming pattern slows down the Walker circulation and suppresses the convection over the MC. An anomalous anticyclone is induced over the northern IO by the negative heating anomaly over MC, and it weakens SASM westerly. Meanwhile, the ocean warming in the tropical and mid-latitude Pacific increases local moisture and convective instability, weakening the NPSH. The weakened NPSH induces an anomalous northerly over EA, weakening EASM southerly.

The combined fast and slow processes lead to a weakening of the monsoon westerly over SA but a strengthening of the monsoon southerly over EA. The main process that strengthens EASM circulation is the fast land warming and associated intensified TP thermal forcing. This differs markedly from the SASM circulation change, which is primarily determined by the SST warming pattern in the equatorial Pacific.

One may wonder why the future change of the monsoon circulation matters. The Indian government has set an ambitious target for future renewable power generation including wind power capacity, and the benefit of the substantial investments depends on the future circulation change [58]. Furthermore, projecting a realistic circulation change is critical for projecting monsoon precipitation change [8,38]. The current state-of-the-art climate models would underestimate the monsoon precipitation change in the future, if a La Niña-like mean state response should occur. Recently there were heated debates and arguments about whether or not the El Niño-like mean state response to global warming might result from the cold tongue bias of the coupled models [59,60]. If the bias is somehow corrected, one could expect a strengthened SASM circulation response, which would greatly increase the monsoon (mean and extreme) precipitation in the future.

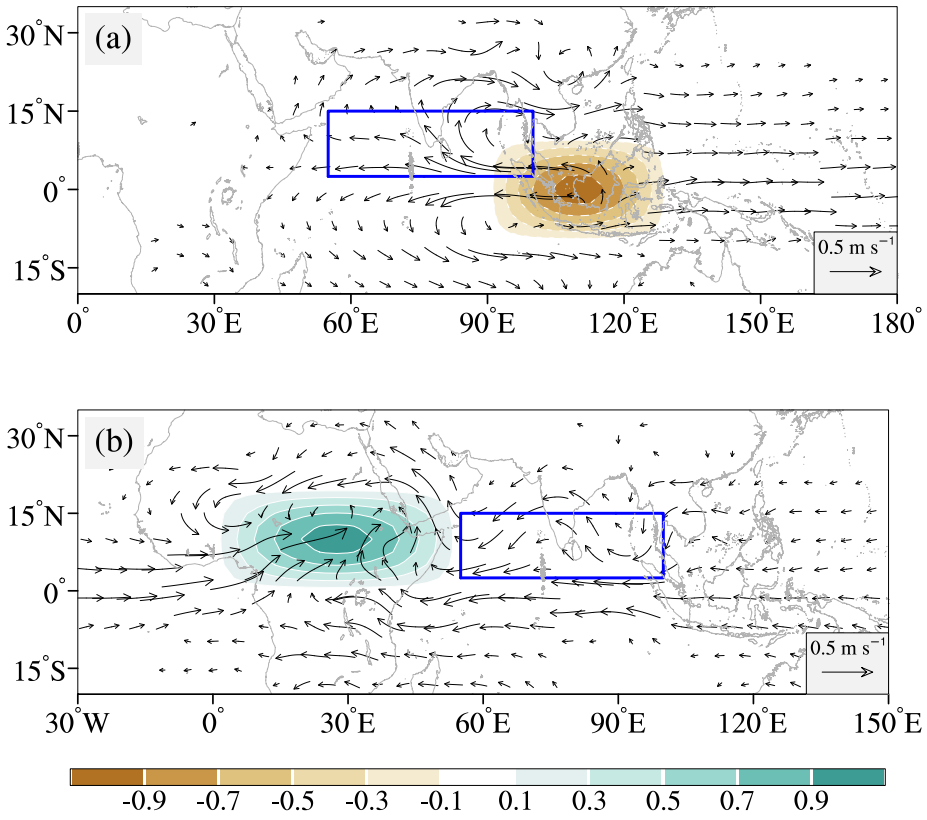

Fig. 5. The response of low-level atmospheric wind field (m s^{-1}) to the prescribed heating anomaly over the Maritime Continent (10°S–10°N, 90°–130°E) (a) and the North Africa (0°–20°N, 0°–55°E) (b) with the maximum heating rate of 1 K d^{-1}. The blue rectangle denotes the SASMI region.

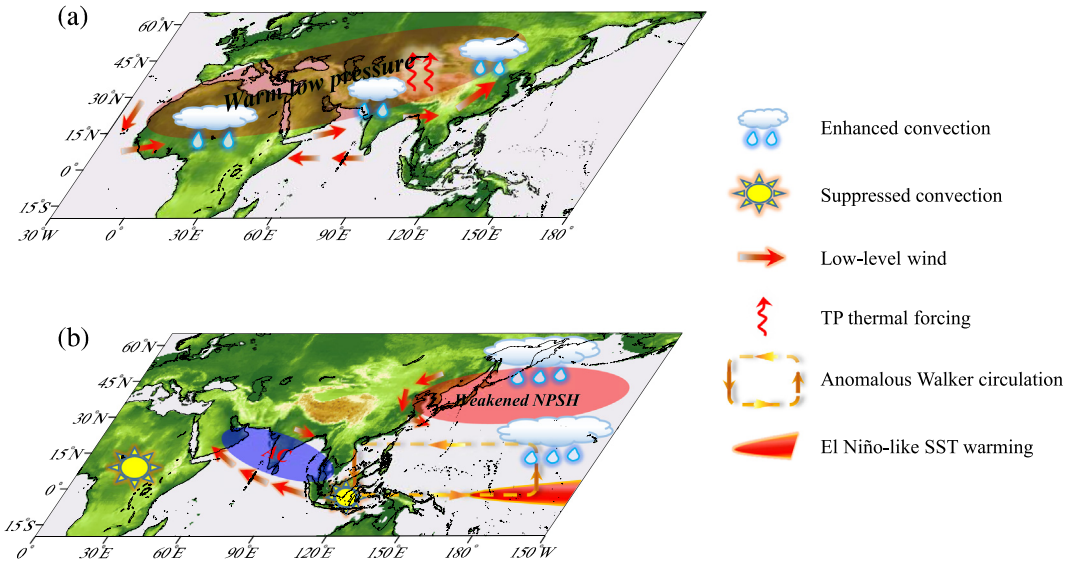

Fig. 6. Schematic diagrams for the mechanisms of the ASM circulation change under global warming through a fast (a) and a slow (b) response. A fast land warming over the Eurasian continent along with the intensified TP thermal forcing induces a large-scale cyclonic circulation, strengthening low-level southerly over EA. Meanwhile, moisture transport by anomalous southwesterly increases rainfall over NA, which weakens the SASM westerly through inducing anomalous easterly. A slow oceanic response is characterized by an El Niño-like warming pattern over the equatorial Pacific, which slows down the Walker circulation and suppresses convection over the MC. The negative heating anomaly over the MC further induces an anomalous anticyclone over the northern IO and weakens the SASM westerly. Meanwhile, the ocean warming in the tropical and mid-latitude Pacific increases local moisture and convective instability, weakening the NPSH. This leads to a weakening of southerly over EA. The fast (slow) process dominates the EASM (SASM) circulation response.

Conflict of interest

All authors declare that they have no conflict of interest.

Acknowledgments

This work was supported by the National Natural Science Foundation of China (42088101), the National Key Research & Development Program of China (2017YFA0603802), and US National Science Foundation (AGS-2006553). This is School of Ocean and Earth Science and Technology contribution number 11429, International Pacific Research Center contribution number 1545 and Earth System Modeling Center contribution number 358.

Author contributions

Tim Li designed the research plan. Yuhao Wang performed the analysis and plotted figures. Tim Li and Yuhao Wang drafted and revised the manuscript. Bin Wang, Mingfang Ting, Yihui Ding, Ying Sun, Chao He and Guang Yang provided the comments and revised the manuscript.

Appendix A. Supplementary materials

Supplementary materials to this article can be found online at https://doi.org/10.1016/j.scib.2021.12.001.

References

[1] Krishnamurti TN. Observational study of the tropical upper tropospheric motion field during the Northern Hemisphere summer. J Appl Meteorol 1971;10:1066–96.
[2] Wang B, LinHo.. Rainy season of the Asian-Pacific summer monsoon. J Clim 2002;15:386–98.
[3] Gadgil S, Rupa Kumar K. The Asian monsoon—Agriculture and economy. In: Wang B, editor. The Asian Monsoon. Berlin: Springer; 2006. p. 651–83.
[4] Intergovernmental Panel on Climate Change. Climate change 2013: the physical science basis. In: Contribution of working group I to the fifth assessment report of the intergovernmental panel on climate change. Cambridge: Cambridge University Press, 2013.
[5] Chou C, Neelin JD, Chen C-A, et al. Evaluating the "rich-get-richer" mechanism in tropical precipitation change under global warming. J Clim 2009;22:1982–2005.
[6] Held IM, Soden BJ. Robust responses of the hydrological cycle to global warming. J Clim 2006;19:5686–99.
[7] Hsu P-C, Li T. Is "rich-get-richer" valid for Indian Ocean and Atlantic ITCZ? Geophys Res Lett 2012;39:L13705.
[8] Li X, Ting M. Understanding the Asian summer monsoon response to greenhouse warming: the relative roles of direct radiative forcing and sea surface temperature change. Clim Dyn 2017;49:2863–80.
[9] Turner AG, Annamalai H. Climate change and the South Asian summer monsoon. Nat Clim Chang 2012;2:587–95.
[10] Zhou S, Huang P, Huang G, et al. Leading source and constraint on the systematic spread of the changes in East Asian and western North Pacific summer monsoon. Environ Res Lett 2019;14:124059.
[11] Lee J-Y, Wang B. Future change of global monsoon in the CMIP5. Clim Dyn 2014;42:101–19.
[12] Wang Y, He C, Li T. Response of the anomalous western North Pacific anticyclone during El Niño mature winter to global warming. Clim Dyn 2020;54:727–40.
[13] Wang Y, He C, Li T. Impact of global warming on the western North Pacific circulation anomaly during developing El Niño. J Clim 2020;33:2333–49.
[14] Dai A, Li H, Sun Y, et al. The relative roles of upper and lower tropospheric thermal contrasts and tropical influences in driving Asian summer monsoons. J Geophys Res Atmos 2013;118:7024–45.
[15] Li C, Yanai M. The onset and interannual variability of the Asian summer monsoon in relation to land–sea thermal contrast. J Clim 1996;9:358–75.
[16] He C, Wang Z, Zhou T, et al. Enhanced latent heating over the Tibetan Plateau as a key to the enhanced East Asian summer monsoon circulation under a warming climate. J Clim 2019;32:3373–88.
[17] Wu G, Liu Y. Impacts of the Tibetan Plateau on Asian climate. Meteorol Monogr 2016;56:7.1–7.29.
[18] Yanai M, Wu G-X. Effects of the Tibetan Plateau. In: Wang B, editor. The Asian Monsoon. Berlin: Springer; 2006. p. 513–49.
[19] Chen X, Zhou T. Distinct effects of global mean warming and regional sea surface warming pattern on projected uncertainty in the South Asian summer monsoon. Geophys Res Lett 2015;42:9433–9.
[20] Li G, Xie S-P, He C, et al. Western pacific emergent constraint lowers projected increase in Indian summer monsoon rainfall. Nat Clim Chang 2017;7:708–12.
[21] Wang B, Clemens SC, Liu P. Contrasting the Indian and East Asian monsoons: implications on geologic timescales. Mar Geol 2003;201:5–21.
[22] Jin C, Wang B, Liu J. Future changes and controlling factors of the eight regional monsoons projected by CMIP6 models. J Clim 2020;33:9307–26.
[23] Menon A, Levermann A, Schewe J, et al. Consistent increase in Indian monsoon rainfall and its variability across CMIP-5 models. Earth Syst Dyn 2013;4:287–300.
[24] Sharmila S, Joseph S, Sahai AK, et al. Future projection of Indian summer monsoon variability under climate change scenario: an assessment from CMIP5 climate models. Glob Planet Change 2015;124:62–78.
[25] Kamae Y, Watanabe M, Kimoto M, et al. Summertime land–sea thermal contrast and atmospheric circulation over East Asia in a warming climate—Part i: past changes and future projections. Clim Dyn 2014;43:2553–68.
[26] Li Z, Sun Y, Li T, et al. Future changes in East Asian summer monsoon circulation and precipitation under 1.5 to 5 °C of warming. Earth Future 2019;7:1391–406.
[27] Byrne MP, O'Gorman PA. Land–ocean warming contrast over a wide range of climates: convective quasi-equilibrium theory and idealized simulations. J Clim 2013;26:4000–16.
[28] Bony S, Bellon G, Klocke D, et al. Robust direct effect of carbon dioxide on tropical circulation and regional precipitation. Nat Geosci 2013;6:447–51.
[29] Mitchell JFB. The seasonal response of a general circulation model to changes in CO_2 and sea temperatures. Q J R Meteorol Soc 1983;109:113–52.
[30] Shaw TA, Voigt A. Tug of war on summertime circulation between radiative forcing and sea surface warming. Nat Geosci 2015;8:560–6.
[31] Cao L, Bala G, Caldeira K. Climate response to changes in atmospheric carbon dioxide and solar irradiance on the time scale of days to weeks. Environ Res Lett 2012;7:034015.
[32] Long S-M, Xie S-P, Zheng X-T, et al. Fast and slow responses to global warming: sea surface temperature and precipitation patterns. J Clim 2014;27:285–99.
[33] Stouffer RJ. Time scales of climate response. J Clim 2004;17:209–17.
[34] Ceppi P, Zappa G, Shepherd TG, et al. Fast and slow components of the extratropical atmospheric circulation response to CO_2 forcing. J Clim 2018;31:1091–105.
[35] Eyring V, Bony S, Meehl GA, et al. Overview of the Coupled Model Intercomparison Project Phase 6 (CMIP6) experimental design and organization. Geosci Model Dev 2016;9:1937–58.
[36] Deser C, Phillips A, Bourdette V, et al. Uncertainty in climate change projections: the role of internal variability. Clim Dyn 2012;38:527–46.
[37] Huang X, Zhou T, Dai A, et al. South Asian summer monsoon projections constrained by the interdecadal Pacific oscillation. Sci Adv 2020;6:eaay6546.
[38] Xie S-P, Deser C, Vecchi GA, et al. Towards predictive understanding of regional climate change. Nat Clim Chang 2015;5:921–30.
[39] He C, Zhou W. Different enhancement of the East Asian summer monsoon under global warming and interglacial epochs simulated by CMIP6 models: role of the subtropical high. J Clim 2020;33:9721–33.
[40] Gleckler PJ, Taylor KE, Doutriaux C. Performance metrics for climate models. J Geophys Res 2008;113:D06104.
[41] Wilks DS. Statistical forecasting. In: Wilks DS, editor. Statistical methods in the atmospheric sciences. Amsterdam: Elsevier; 2019. p. 235–312.
[42] Kanamitsu M, Ebisuzaki W, Woollen J, et al. NCEP-DOE AMIP-II Reanalysis (R-2). Bull Amer Meteorol Soc 2002;83:1631–44.
[43] Adler RF, Huffman GJ, Chang A, et al. The version-2 global precipitation climatology project (GPCP) monthly precipitation analysis (1979–present). J Hydrometeorol 2003;4:1147–67.
[44] Webster PJ, Yang S. Monsoon and ENSO: selectively interactive systems. Q J R Meteorol Soc 1992;118:877–926.
[45] Wang B, Wu R, Lau K-M. Interannual variability of the asian summer monsoon: contrasts between the Indian and the western North Pacific-East Asian monsoons. J Clim 2001;14:4073–90.
[46] Guo Q. The summer monsoon index in East Asia and its variation. Acta Geogr Sin 1983;38:208–17 (in Chinese).
[47] Wang B, Wu Z, Li J, et al. How to measure the strength of the East Asian summer monsoon. J Clim 2008;21:4449–63.
[48] Held IM, Suarez MJ. A proposal for the intercomparison of the dynamical cores of atmospheric general circulation models. Bull Amer Meteorol Soc 1994;75:1825–30.
[49] Jiang X-A, Li T. Reinitiation of the boreal summer intraseasonal oscillation in the tropical Indian Ocean. J Clim 2005;18:3777–95.
[50] Li T. Origin of the summertime synoptic-scale wave train in the western North Pacific. J Atmos Sci 2006;63:1093–102.
[51] Gill AE. Some simple solutions for heat-induced tropical circulation. Q J R Meteorol Soc 1980;106:447–62.
[52] Wu G, Liu Y, Zhang Q, et al. The influence of mechanical and thermal forcing by the Tibetan Plateau on Asian climate. J Hydrometeorol 2007;8:770–89.
[53] Hill SA. Theories for past and future monsoon rainfall changes. Curr Clim Chang Rep 2019;5:160–71.
[54] Seth A, Giannini A, Rojas M, et al. Monsoon responses to climate changes—Connecting past, present and future. Curr Clim Chang Rep 2019;5:63–79.
[55] Zhang L, Li T. A simple analytical model for understanding the formation of sea surface temperature patterns under global warming. J Clim 2014;27:8413–21.
[56] Zhang L, Li T. Relative roles of differential SST warming, uniform SST warming and land surface warming in determining the Walker circulation changes under global warming. Clim Dyn 2017;48:987–97.

[57] Wang B, Wu R, Li T. Atmosphere–warm ocean interaction and its impacts on Asian-Australian monsoon variation. J Clim 2003;16:1195–211.
[58] Gao M, Ding Y, Song S, et al. Secular decrease of wind power potential in India associated with warming in the Indian Ocean. Sci Adv 2018;4:eaat5256.
[59] Coats S, Karnauskas KB. Are simulated and observed twentieth century tropical Pacific sea surface temperature trends significant relative to internal variability? Geophys Res Lett 2017;44:9928–37.
[60] Seager R, Cane M, Henderson N, et al. Strengthening tropical Pacific zonal sea surface temperature gradient consistent with rising greenhouse gases. Nat Clim Chang 2019;9:517–22.

Tim Li is Professor of Atmospheric Sciences at Department of Atmospheric Sciences and International Pacific Research Center, University of Hawaii at Manoa. His general research interest is tropical meteorology, climate dynamics, atmosphere-ocean interaction and numerical weather prediction. The current research topics include: (1) Dynamics of ENSO and inter-basin teleconnection, (2) Asian-Australian monsoon and Tropospheric Biennial Oscillation, (3) climate changes under global warming, (4) Madden-Julian oscillation, (5) tropical cyclone, and (6) multi-scale Eddy-mean flow interaction.